



I S A V

**Journal of Theoretical and Applied
Vibration and Acoustics**

journal homepage: <http://tava.isav.ir>



The effect of distance and dimensions of magnets on nonlinear behavior of piezomagnetoelastic bimorph energy harvester

Heshmatolah Mohammad Khanlo^a, Reza Dehghani^{b*}

^a Assistant Professor, Department of Aerospace Engineering, Shahid Sattari Aeronautical University of Science and Technology, Tehran, Iran

^b Assistant Professor, Faculty of Mechanical and Material Engineering, Graduate University of Advanced Technology, Kerman, Iran

ARTICLE INFO

Article history:

Received 27 November 2017

Received in revised form
1 June 2018

Accepted 20 June 2018

Available online 29 June 2018

Keywords:

Bimorph

Energy harvesting

Piezoelectric layers

Magnet

Bifurcation

ABSTRACT

This paper presents the effect of distance and dimensions of magnets on chaotic behavior and voltage level of a vibratory piezo-magneto-elastic bimorph energy harvesting system. The bimorph model comprises two piezoelectric layers on a cantilever base structure with one tip magnet as well as two external magnets. The mathematical model is extracted by using distributed model. The validity of the extracted model verified by previously published experimental results. In order to study the nonlinear dynamic of the bimorph, bifurcation diagram, phase plane portrait, time history response, Poincare map, power spectra diagram, and maximum Lyapunov exponents are used. In the bifurcation diagrams, the control parameters are the distances and dimensions of the magnets. It is shown that in the specific region of the control parameters, the sub-harmonic or super-harmonic behavior has minimum harvested voltage and irregular regions has maximum voltage. Also specific dimensions of tip magnet can influence greatly the dynamic behavior as well as output voltage. So these obtained results can give good insights about parameters identification and realization of the nonlinear behavior to reach the broadband higher harvested voltage of the system.

© 2018 Iranian Society of Acoustics and Vibration, All rights reserved.

1. Introduction

In two current decades the energy harvesting systems that convert a natural ambient energy to electricity has been an attractive research area. Energy harvesting systems mainly rely on the physics of piezoelectric materials and electromagnetic induction to convert ambient mechanical energy to electrical energy. There are various methods and applications for energy harvesting

* Corresponding author:

E-mail address: R.dehghani@kgut.ac.ir (R. Dehghani)

<http://dx.doi.org/10.22064/tava.2018.76308.1091>

systems. Some of the significant applications include mechanical impact [1], drilling operations in deep and ultra-deep wells[2], micro-electro-mechanical sensors [3], velocity amplification in electromagnetic shock absorbers[4, 5], aero elastic [6] and other applications[7-9], that are introduced in references. Among these, the vibratory energy harvesting systems has been significant research area, due to its various applications and scientific challenges. The main purpose in this way is to supply the required electrical energy for various requirements by using the vibration energy of the environment. There are three methods to convert the vibrations to electrical energy; that are the electrostatic, the electromagnetic [10] and the piezoelectric transductions [11]. In recent years, the piezoelectric transduction has the greatest attention. Usually the vibratory piezoelectric energy harvesters are in the form of unimorph and bimorph cantilever beams configuration. The main structure of the harvester is located on a vibrating base and the dynamic strain induced in piezoelectric layers results in an alternate voltage across their electrodes. Also, piezo-magneto-elastic configuration over piezoelastic configuration is preferred, due to its higher output voltage in all excitation frequencies except resonant frequency.

However, appropriate mathematical model of the vibratory energy harvesting systems is a main challenging issue. Proper mathematical model that realize the physical characteristics, can result in reliable responses in the simulation process. In the early mathematical models, lumped parameter model with a one degree of freedom (d.o.f) is used [12, 13] to investigate the system dynamic behavior. Although the lumped model gives some initial knowledge into the problem, but it is an approximate model and it lacks some important aspects such as the mode shapes and exact strain distribution and their effects on electric response of the real physical system. The Rayleigh-Ritz model [3, 14, 15] is as an improved modeling approach, gives a discretized model of the distributed system that has a more exact approximation compared to lumped modeling with one d.o.f; but it is more computationally expensive than analytical solution. The analytical methods based on distributed electromechanical model and experimental verifications [16-18] and finite element [19, 20] simulations are given as accurate models. Zhao et al.[21] presented the modeling approach based on a distributed-parameter electro-elastic formulation to ensure that the effects of higher vibration modes are included.

Some works focused on exploiting the mechanical nonlinearities in vibratory energy harvesters and modifying the linear models to improve the broadband energy harvesting performance. Stanton et al.[22] show that, proper liability of nonlinearities in the physical models can be used to effectively capture the experimental observed responses. Also Abdelkefi et al. [23] developed a global nonlinear distributed model of a piezoelectric energy harvester with parametric excitation and indicate that the nonlinear distributed model by considering the first three modes has better response than the lumped-parameter method for designing the energy harvester. Analysis and simulations have been performed by Ferrari et al.[24, 25] showed that a higher amount of energy extracted from nonlinear converter in comparison to a linear one and nonlinear bi-stable harvester has better performances with wideband excitation in comparison to the linear system.

In the nonlinear energy harvesters, increasing the performance and enhancement of frequency bandwidth is the other research issue has been focused by some researchers [26-34].

In some researches, the magnet forces have used for improving efficiency of the energy harvester. Cao et al.[35] show by experimental test and numerical analysis that the lumped parameters equations with identified polynomials for magnetic force could sufficiently describe

the specialties of the nonlinear energy harvester. Stanton et al. [22] derived a full nonlinear model with an analytical magnet formulation and proper modal expressions to account for discontinuous piezoelectric laminates. Their results showed that proper separation distance of the magnets could be determined by studying the magnet spacing as a bifurcation parameter. Caruso et al. [36] proposed an adaptive electromagnetic energy harvester that comprises a vibrating mass an electromagnetic transducer and resonant resistive– capacitive– inductive electric circuit for increase its effective bandwidth. Firoozy et al.[37] investigated the dynamic behavior of the uni-morph piezoelectric beam with tip magnets. Influence of some parameters on behavior of system and output power has been studied. Yildirim et al. [38, 39] studied effect of restoring-electromagnetic couplings on the frequency bandwidth.

In the nonlinear systems, the chaos is a phenomenon that can be occurred in some conditions. By including the chaotic behavior as a favorable property, small disturbances can change the behavior of the system exceedingly. So by this property one can improve the dynamic response of the energy harvesters. Geiyer and Kauffman[40] showed that the bandwidth of power output can increase by inducing chaotic behaviors and applying the low power controller. Thereby, by handling the motion to a chaotic attractor, even excitations with single frequency can results in an infinite number of periodic orbits that theoretically can be stabilized by using small controller inputs.

However, literature reviews showed that some researches[10, 22, 27, 28, 30] have been developed to exploit chaotic behaviors in the energy harvesting systems but many aspects of this phenomenon still need to investigation precisely. The main contribution of this paper is nonlinear analysis of a typical piezo-magneto-elastic bimorph energy harvesting system based on dynamic model derived by the

2. Mathematical modeling of piezo-magneto-elastic bimorph

As shown in Fig. 1, the proposed system is including of a bimorph cantilever and three magnets, where the one magnet is attached to the tip of the beam, and two external magnets are connected on a fixed frame of the system. The magnetization of the tip magnet is in negative vertical direction, and the magnetizations of two external magnets are in positive vertical direction; so, it can result in magnetic force and moment on the beam's tip. This magnetic effect can be defined as a relative positions of the three magnets, which specified by two distances: (1) the separation distance d_x between the external magnets and tip magnet and (2) the gap distance between external magnets, d_z .

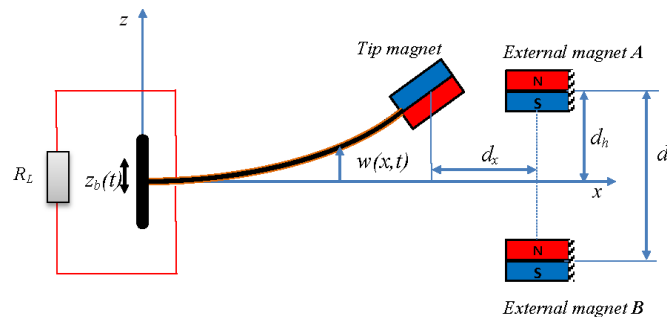


Fig. 1. Schematic of a typical piezo-magneto-elastic bimorph energy harvesting system.

The displacement vector of beam element can be written as [11]

$$\mathbf{p}_r = -zw' \mathbf{i} + w \mathbf{k} \quad (1)$$

where $w = w(x, t)$ is the lateral displacement and z is the vertical distance from the beam neutral axis.

The velocity vector of the beam element is

$$\dot{\mathbf{p}} = -z\dot{w}' \mathbf{i} + (\dot{w} + \dot{z}_b) \mathbf{k} \quad (2)$$

where \dot{z}_b is the base velocity; the dot symbol ($\dot{}$) and the prime symbol ($'$) define differentiation with respect to time and displacement x , respectively. The kinetic energy of the bimorph beam can be obtained by

$$T = \frac{1}{2} \int_{V_s} \rho_s \dot{\mathbf{p}}^T \dot{\mathbf{p}} dV_s + \frac{1}{2} \int_{V_{p_1}} \rho_p \dot{\mathbf{p}}^T \dot{\mathbf{p}} dV_{p_1} + \frac{1}{2} \int_{V_{p_2}} \rho_p \dot{\mathbf{p}}^T \dot{\mathbf{p}} dV_{p_2} + \frac{1}{2} M \dot{\mathbf{p}}_M^T \dot{\mathbf{p}}_M + \frac{1}{2} I_M \dot{w}'^2 \quad (3)$$

where the subscript 's' is for the beam substructure; the subscript 'p' is for the piezoelectric layers such that 'p₁' and 'p₂' denote the lower and upper piezoelectric layers, respectively; the subscript 'M' is for the tip magnet. Also, ρ_i ($i = s, p$) is the mass density, M , I_M and $\dot{\mathbf{p}}_M$ are the mass, the moment of inertia and the velocity vector of the tip magnet, respectively. The axial strain component can be expressed as

$$\varepsilon_{xx} = \frac{\partial \mathbf{p}_r}{\partial x} \cdot \mathbf{i} = \frac{\partial}{\partial x} (-zw') = -zw'' \quad (4)$$

By Hooke's law the axial stress of the substructure is given as

$$\sigma_{xx}^s = E_s \varepsilon_{xx} = E_s (-zw'') \quad (5)$$

where E_s is the beam Young modulus.

If the piezoelectric layer's behavior is modeled as a thin beam on the basis of the Euler–Bernoulli beam theory, the components of stress can be regarded as the one-dimensional bending stress. Therefore, the stress–electric displacement in the reduced form constitutive equations for a mentioned above beam is [11]

$$\sigma_{xx}^p = E_p \varepsilon_{xx} - e_{31} E_3 = E_p (-zw'') - e_{31} E_3 \quad (6)$$

where E_p is the piezoelectric layer modulus of elasticity; e_{31} is the stress constant of piezoelectric. The electric field E_3 is given in terms of the output voltage for the bimorph piezoelectric layer [11] as

$$E_3 = \frac{-v(t)}{2h_p} \quad (7)$$

where $v(t)$ is the voltage between the electrodes and h_p is the piezoelectric layers thickness. Also, the bimorph potential energy is given by

$$U = \frac{1}{2} \int_{V_s} E_s \varepsilon_{xx}^2 dV_s + \frac{1}{2} \int_{V_{p1}} (E_p \varepsilon_{xx} - e_{31} E_3) \varepsilon_{xx} dV_{p1} + \frac{1}{2} \int_{V_{p2}} (E_p \varepsilon_{xx} - e_{31} E_3) \varepsilon_{xx} dV_{p2} \quad (8)$$

The internal electrical energy of the piezoelectric layers is obtained as

$$\begin{aligned} W_e &= W_{e_1} + W_{e_2} \\ &= \frac{1}{2} \int_{V_{p1}} \mathbf{E}^T \mathbf{D} dV_{p1} + \frac{1}{2} \int_{V_{p2}} \mathbf{E}^T \mathbf{D} dV_{p2} \\ &= \frac{1}{2} \int_{V_{p1}} E_3 (e_{31} \varepsilon_{xx} + \varepsilon_{33}^s E_3) dV_{p1} + \frac{1}{2} \int_{V_{p2}} E_3 (e_{31} \varepsilon_{xx} + \varepsilon_{33}^s E_3) dV_{p2} \end{aligned} \quad (9)$$

where \mathbf{E} is the vector of electric field and \mathbf{D} is the vector of electric displacement (dielectric) that are defined as

$$\begin{aligned} \mathbf{E} &= [0 \quad 0 \quad E_3]^T \\ \mathbf{D} &= [0 \quad 0 \quad D_3]^T \end{aligned} \quad (10)$$

where $D_3 = e_{31} \varepsilon_{xx} + \varepsilon_{33}^s E_3$; ε_{33}^s is the permittivity component at constant strain with the plane stress assumption for a beam.

When the base of the bimorph cantilever beam is harmonically excited, the beam deforms and oscillates, and so the tip magnet to have a tendency to travel in the field of external magnets [41]. Consequently, we need to first determine the magnetic flux density generated by the two external magnets. Since the magnet's dimensions used in this work are small compare to the field's dimensions, the magnets are modeled as point dipoles, [22, 42]. So the magnetic force and moment can be calculated in usual form. The thin rectangular shaped tip magnetization is used here and linear/saturated magnetization model is applied[41, 43]. The following assumptions are made here:

- 1- The hysteresis effect of magnetization is neglected.
2. Since the size of the tip magnet is small, so the magnetic characteristics within the body of tip magnet are uniform.

After determining of the magnetization of the tip magnet by exerting an external field, the magnetic force and moment on tip magnet can obtain in usual method for permanent magnets. In this work, the tip magnet and two external magnets are modeled as a charge model, where a magnet is reduced to a distribution of equivalent magnetic charges and also point dipole approximation is invoked for all magnets[44].

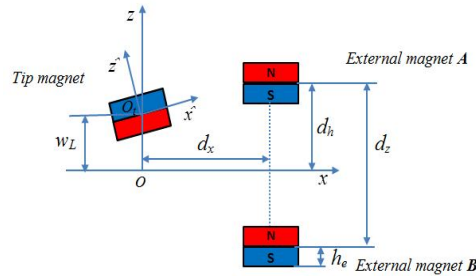


Fig. 2 Schematic of the tip magnet and two external magnets.

Based on schematic shown in Fig. 2 and aforementioned assumptions, the magnetic forces and moment are obtained using a series of derivation process[45]

$$f_{M_x} = -\frac{\mu_0 M_t M_e}{4\pi} \sum_{i,j,k=1,2} (-1)^{j+k} \frac{X_x^{(k)}}{(X_x^{(k)^2} + X_z^{(i,j,k)^2})^{1.5}} \quad (11)$$

$$f_{M_z} = -\frac{\mu_0 M_t M_e}{4\pi} \sum_{i,j,k=1,2} (-1)^{j+k} \frac{X_z^{(i,j,k)}}{(X_x^{(k)^2} + X_z^{(i,j,k)^2})^{1.5}} \quad (12)$$

$$\tau_M = -\frac{\mu_0 M_t M_e}{4\pi} \sum_{i,j,k=1,2} (-1)^{j+k} \frac{R_y^{(i,j,k)}}{(X_x^{(k)^2} + X_z^{(i,j,k)^2})^{1.5}} \quad (13)$$

$$d_h^{(i,j,k)} = (-1)^i d_h - (-1)^j h_e + (-1)^k h_t \quad (14)$$

$$h_t^{(k)} = (-1)^k h_t \quad (15)$$

$$X_x^{(k)} = -h_t^{(k)} w'_L - d_x \quad (16)$$

$$X_z^{(i,j,k)} = w_t + l_t w'_L + d_h^{(i,j,k)} \quad (17)$$

$$R_y^{(i,j,k)} = -\left[l_t - h_t^{(k)} w'_L \right] X_z^{(i,j,k)} + \left[l_t w'_L + h_t^{(k)} \right] X_x^{(k)} \quad (18)$$

where $d_h = \frac{d_z}{2}$ and μ_0 is the free space permeability; M_t and M_e are the tip magnet and two external magnets total surface charges, respectively; h_t and h_e are the tip magnet and the external magnets half-heights, respectively. l_t is the tip magnet length, w_t is the tip magnet lateral displacements and w'_L is the tip magnet slope with respect to horizontal axis.

The non-conservative mechanical force and electric charge components are as a generalized force that be considered by virtual work as

$$\delta W_{nc} = f_E(t) \delta v + f_{M_z} \delta w_L + \tau_M \delta w'_L \quad (19)$$

where $f_E(t) = \int_0^t \frac{v}{R_L} dt$ is the output electric charge of the piezoelectric layers; τ_M and f_{M_z} are the magnetic moment and force, respectively. Also w_L and w'_L are given as follows.

$$w_L = w(L, t), \quad w'_L = \left. \frac{\partial w(x, t)}{\partial x} \right|_{x=L} \quad (20)$$

The $w(x, t)$ is the mechanical domain distributed-parameter variable, and $v(t)$ is the electrical variable. In order to obtain the discretized differential equations of motion, we used assumed mode method. To this end, the following finite series is considered for $w(x, t)$.

$$w(x, t) = \sum_{j=1}^n \psi_j(x) q_j(t) \quad (21)$$

where $\psi_j(x) = A_j (1 - \cos[(2j - 1)\pi x / (2L)])$ is the admissible trial function which satisfy the essential boundary conditions, $q_j(t)$ is the unknown generalized coordinate, and n is the modes number that considered for the solution.

Using Eq. (21), the kinetic, the potential and the electric energies are given as

$$\begin{aligned}
 T = & \frac{1}{2} \int_{V_s} \rho_s z^2 \sum_{i=1}^n \sum_{j=1}^n \psi_i'(x) \psi_j'(x) \dot{q}_i \dot{q}_j dV_s + \frac{1}{2} \int_{V_s} \rho_s \sum_{i=1}^n \sum_{j=1}^n \psi_i(x) \psi_j(x) \dot{q}_i \dot{q}_j dV_s \\
 & + \int_{V_s} \rho_s \sum_{j=1}^n \psi_j(x) \dot{q}_j \dot{z}_b dV_s + \frac{1}{2} \int_{V_s} \rho_s \dot{z}_b^2 dV_s + \frac{1}{2} \int_{V_{p_1}} \rho_p z^2 \sum_{i=1}^n \sum_{j=1}^n \psi_i'(x) \psi_j'(x) \dot{q}_i \dot{q}_j dV_{p_1} \\
 & + \frac{1}{2} \int_{V_{p_1}} \rho_p \sum_{i=1}^n \sum_{j=1}^n \psi_i(x) \psi_j(x) \dot{q}_i \dot{q}_j dV_{p_1} + \int_{V_{p_1}} \rho_p \sum_{j=1}^n \psi_j(x) \dot{q}_j \dot{z}_b dV_{p_1} + \frac{1}{2} \int_{V_{p_1}} \rho_p \dot{z}_b^2 dV_{p_1} \\
 & + \frac{1}{2} \int_{V_{p_2}} \rho_p z^2 \sum_{i=1}^n \sum_{j=1}^n \psi_i'(x) \psi_j'(x) \dot{q}_i \dot{q}_j dV_{p_2} + \frac{1}{2} \int_{V_{p_2}} \rho_p \sum_{i=1}^n \sum_{j=1}^n \psi_i(x) \psi_j(x) \dot{q}_i \dot{q}_j dV_{p_2} \\
 & + \int_{V_{p_2}} \rho_p \sum_{j=1}^n \psi_j(x) \dot{q}_j \dot{z}_b dV_{p_2} + \frac{1}{2} \int_{V_{p_2}} \rho_p \dot{z}_b^2 dV_{p_2} + \frac{1}{2} M \left[\sum_{i=1}^n \sum_{j=1}^n \psi_i(L) \psi_j(L) \dot{q}_i \dot{q}_j \right. \\
 & \left. + 2 \sum_{i=1}^n \psi_i(L) \dot{q}_i \dot{z}_b + \dot{z}_b^2 \right] + \frac{1}{2} I_M \sum_{i=1}^n \sum_{j=1}^n \psi_i'(L) \psi_j'(L) \dot{q}_i \dot{q}_j
 \end{aligned} \tag{22}$$

$$\begin{aligned}
 U = & \frac{1}{2} \int_{V_s} E_s \left(z^2 \sum_{i=1}^n \sum_{j=1}^n \psi_i''(x) \psi_j''(x) q_i q_j \right) dV_s + \frac{1}{2} \int_{V_{p_1}} E_p \left(z^2 \sum_{i=1}^n \sum_{j=1}^n \psi_i''(x) \psi_j''(x) q_i q_j \right) dV_{p_1} \\
 & - \frac{1}{2} \int_{V_{p_1}} e_{31} E_3 \left(-z \sum_{j=1}^n \psi_j''(x) q_j \right) dV_{p_1} + \frac{1}{2} \int_{V_{p_2}} E_p \left(z^2 \sum_{i=1}^n \sum_{j=1}^n \psi_i''(x) \psi_j''(x) q_i q_j \right) dV_{p_2} \\
 & - \frac{1}{2} \int_{V_{p_2}} e_{31} E_3 \left(-z \sum_{j=1}^n \psi_j''(x) q_j \right) dV_{p_2}
 \end{aligned} \tag{23}$$

$$\begin{aligned}
 W_e = & \frac{1}{2} \int_{V_{p_1}} E_3 e_{31} \left(-z \sum_{j=1}^n \psi_j'' q_j \right) dV_{p_1} + \frac{1}{2} E_3^2 \epsilon_{33}^s V_{p_1} \\
 & + \frac{1}{2} \int_{V_{p_2}} E_3 e_{31} \left(-z \sum_{j=1}^n \psi_j'' q_j \right) dV_{p_2} + \frac{1}{2} E_3^2 \epsilon_{33}^s V_{p_2}
 \end{aligned} \tag{24}$$

Eqs. (22) to (24) rewrite in terms of the matrices defined in Appendix (A) as

$$T = \frac{1}{2} \sum_{i,j=1}^n M_{ij} \dot{q}_i \dot{q}_j + \sum_{i=1}^n H_i \dot{q}_i \dot{z}_b + \frac{1}{2} m_t \dot{z}_b^2 \tag{25}$$

$$U = \frac{1}{2} \sum_{i,j=1}^n K_{ij} q_i q_j + \sum_{i=1}^n E_3 G_i q_i \tag{26}$$

$$W_e = -\sum_{i=1}^n E_3 G_i q_i + \frac{1}{2} E_3^2 \epsilon_{33}^s (V_{p_1} + V_{p_2}) \quad (27)$$

The Lagrange equations based on the extended Hamilton's principle for electromechanical systems are given as

$$\begin{aligned} \frac{d}{dt} \left(\frac{\partial T}{\partial \dot{q}_i} \right) - \frac{\partial T}{\partial q_i} + \frac{\partial U}{\partial q_i} - \frac{\partial W_e}{\partial q_i} &= Q_F \quad (i=1, 2, \dots, n) \\ \frac{d}{dt} \left(\frac{\partial T}{\partial \dot{v}} \right) - \frac{\partial T}{\partial v} + \frac{\partial U}{\partial v} - \frac{\partial W_e}{\partial v} &= Q_E \end{aligned} \quad (28)$$

where Q_E and Q_F are the output electric charge of the piezoelectric layers, the generalized forces, respectively.

The discretized form of the partial differential equations of current electromechanical system are introduced as

$$\begin{aligned} \mathbf{M}\ddot{\mathbf{q}} + \mathbf{K}\mathbf{q} + 2E_3\mathbf{G} + \mathbf{H}\dot{z}_b &= f_{M_z} \boldsymbol{\Psi}(L) + \tau_M \boldsymbol{\Psi}'(L) \\ \frac{C_p}{2} \dot{v} + \frac{v}{R_L} - \frac{1}{h_p} \mathbf{G}^T \dot{\mathbf{q}} &= 0 \end{aligned} \quad (29)$$

where $C_p = \frac{1}{2h_p^2} \epsilon_{33}^s (V_{p_1} + V_{p_2})$ is the equivalent capacitance of the bimorph beam. It should be noted that Eq. (31) is nonlinear, due to generalized forces of the system that arise from magnetic forces and moment.

3. Nonlinear analysis

In the continuous systems the number of assumed modes is more significance, so before conducting the main nonlinear analysis, the number of modes effects on frequencies is investigated. The obtained results have been illustrated in the table 1

This analysis shows that, by increasing the number of modes the estimation of first frequency (50.25 Hz) has not been improved further. Since the exciting frequency of the current system is 10 Hz, that is lower than the first frequency, so the nonlinear analysis conducted by choosing only one mode. However, if the exciting frequency is higher than the first frequency, there is needed to consider higher mode numbers.

Before conducting the numerical analysis for proposed continuous model, the validity of model verified by previously published experimental results. The validity of bimorph, that composed of the main base structure and two upper and lower piezoelectric layers, is performed by the experimental result of reference [22]. The harvested steady state voltage versus amplitude of the exciting force for current model and the experimental result are being compared. As shown in Fig. 3(a), there is good accordance, especially in lower amplitudes (about 0.2 for current model), between two results. The validity of magnetic forces comprises the tip magnet and two external magnets of the current model are verified by the experimental result of reference [35]. The magnetic forces versus vertical displacement of tip magnet are plotted in Fig. 3(b) which reveals

the good accordance between the current model and the experimental result. So, it can be relying on the proposed dynamic model and equations of motion.

Table 1: The effect of the number of modes on the first and second natural frequency

Number Of modes	1Mode		2Mode		3Mode		4Mode		5Mode		6Mode	
	first	second										
Frequency (Hz)	50.25		50.25	445.4	50.25	425.4	50.25	400.4	50.25	395.4	50.25	390.4
Voltage FRF	3.67		3.64	38.6	3.75	29.55	3.76	30.25	3.78	36.45	0.729	11.54

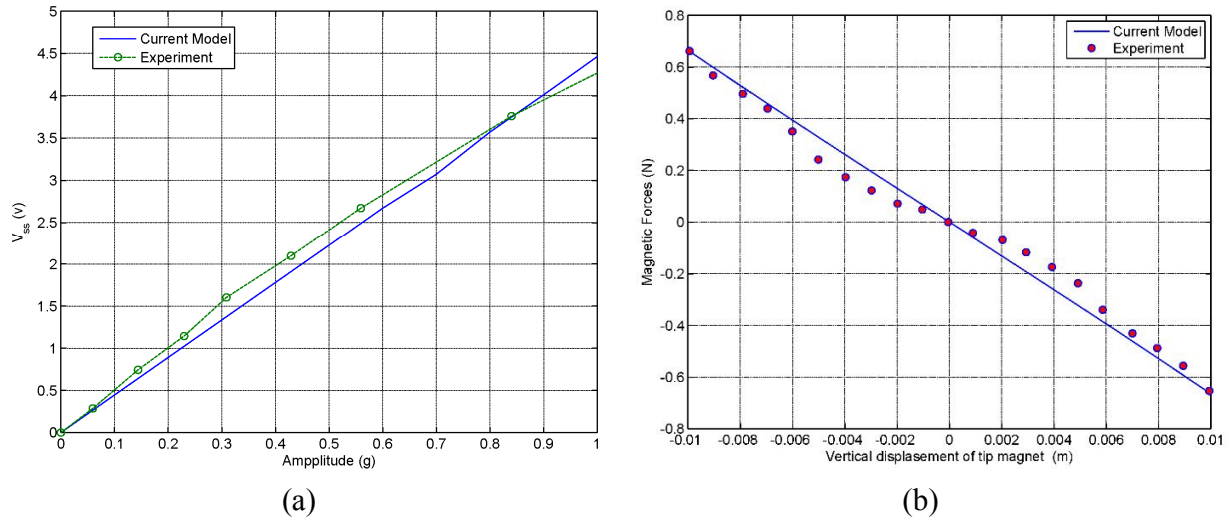


Fig. 3 Dynamic model verification of (a) bimorph, (b) magnetic forces.

The numerical analysis of the equations of motion, Eq. (31), is carried out by the forth-order Runge–Kutta numerical method in MATLAB software. For guarantee the steady state data to perform the nonlinear analysis, the first few hundred captured data’s of numerical analysis were neglected and the results of the next data’s were kept to carry out the numerical analysis. The energy harvesting system parameters used in the numerical study are shown in Table 2. The base acceleration is considered with the frequency 10Hz and the amplitude 2m/s^2 as the system excitation in all numerical simulations. The nonlinear analysis is conducted in two following cases:

3.1. Effect of external magnets distances

To studying the nonlinear dynamic of the system by numerical methods, some identifying techniques are required. One of the main tools to analyze the nonlinear dynamic behavior of the systems is the bifurcation diagrams. The bifurcation diagram can be useful in detecting irregular regions (quasi-periodic or chaotic) of the system behavior under some parameters. In this case, the bifurcation diagrams of the system are obtained by changing the d_z and d_x .

Table2. Parameters value and description

Parameters value	Description
$L = 100\text{mm}$	Beam Length
$b = 6.4\text{mm}$	Beam Width
$h_s = 0.14\text{mm}$	Beam thickness
$\rho_s = 9000\text{kg} / \text{m}^3$	Beam mass density
$E_s = 105\text{Gpa}$	Beam Young's modules
$h_p = 0.265\text{mm}$	Piezoelectric layers thickness
$\rho_p = 7500\text{kg} / \text{m}^3$	Piezoelectric layers Mass density
$e_{31} = -16.6\text{C} / \text{m}^2$	Piezoelectric constant
$\epsilon_{33}^s = 25.55\text{nF} / \text{m}$	Permittivity
$E_p = 60.6\text{Gpa}$	Piezoelectric layers Young's modules
$\rho_M = 7400\text{kg} / \text{m}^3$	Mass density of the tip magnet
$\mu_0 = 4\pi \times 10^{-7}\text{N} / \text{A}^2$	Magnetic constant

Fig. 4 illustrates the bifurcation diagrams of the bimorph beam tip displacement and harvested voltage versus gap distance d_z between the two external magnets. The dominant dynamic behavior of system is the quasi-periodic on the broad region of the parameter changes. However, on some regions can be detected periodic or sub harmonic behaviors. Up to $d_z = 0.137\text{m}$ the beam tip displacements and harvested voltage are not considerable. At the gap distance $d_z = 0.138\text{m}$ both the tip displacements and voltage begin to increase up to $d_z = 0.177\text{m}$. Hereafter, the tip displacement decrease gradually, but the voltage value has sudden lost. After $d_z = 0.178\text{m}$ the tip displacement has some fluctuations up to the end of the region.

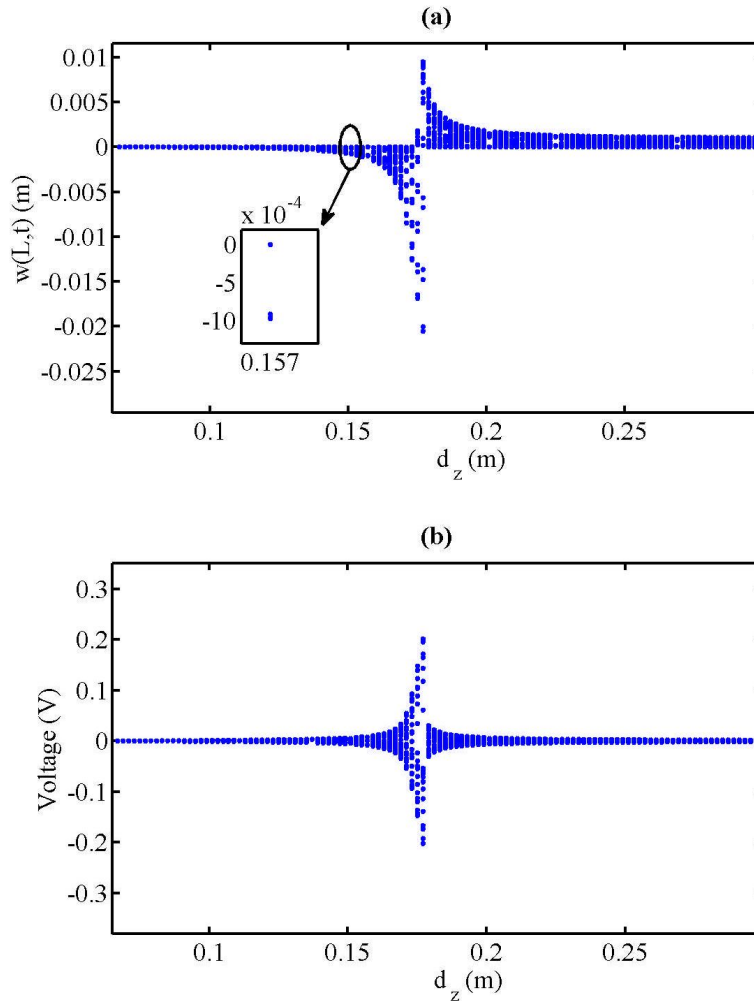


Fig. 4. Bifurcation diagrams (a) beam tip displacement, (b) voltage.

By means of the bifurcations diagram, the overall nonlinear behavior for the system can be identified; but for detail analysis, there is need to other identifying techniques. So the other detection techniques such as time history, phase plane, Poincare map and power spectrum is used to confirm the captured behavior in the bifurcation diagrams. Fig. 5, exhibit the behavior of the system at $d_z = 0.157$ m. The time history has two detectible amplitude and Poincare map has three points; also the power spectrum has an evident peak amplitude after main frequency, that confirm the super-harmonic motion with period three (3T). Fig. 6, shows the typical behavior of the harvesting system at $d_z = 0.177$ m. When the phase plane show many crossing and loops that can be a sign of irregular, quasi-periodic or chaotic motion. Since the time history has some definite but not countable peak and Poincare map is closed curve as well as the power spectrum has some clear peaks, the system behavior is the quasi-periodic. It should be noted that in this case the dominant behavior in the irregular regions is quasi-periodic.

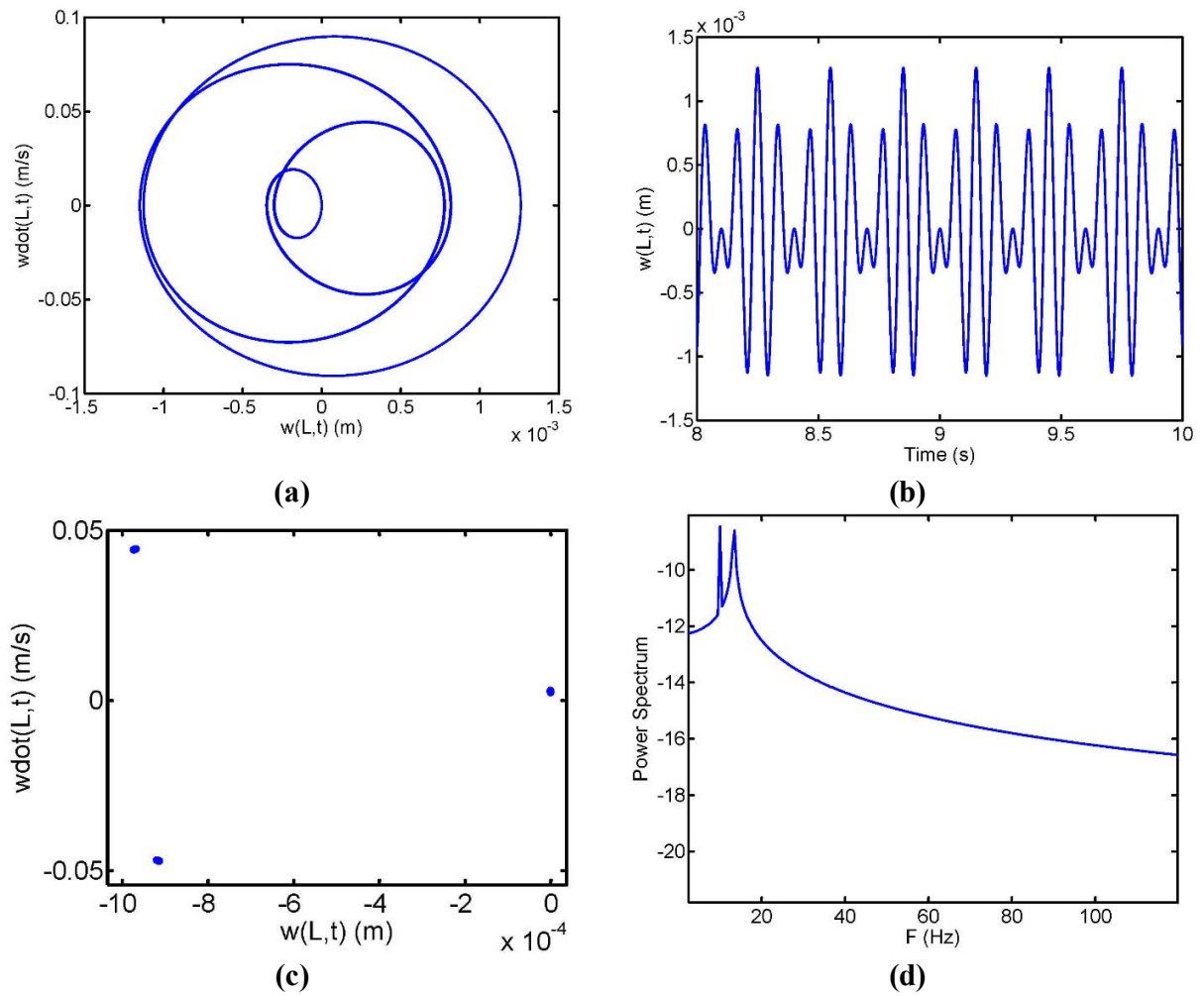


Fig. 5. (a) phase plane, (b) time history, (c) Poincare map, (d) power spectrum for $d_z = 0.157 m$.

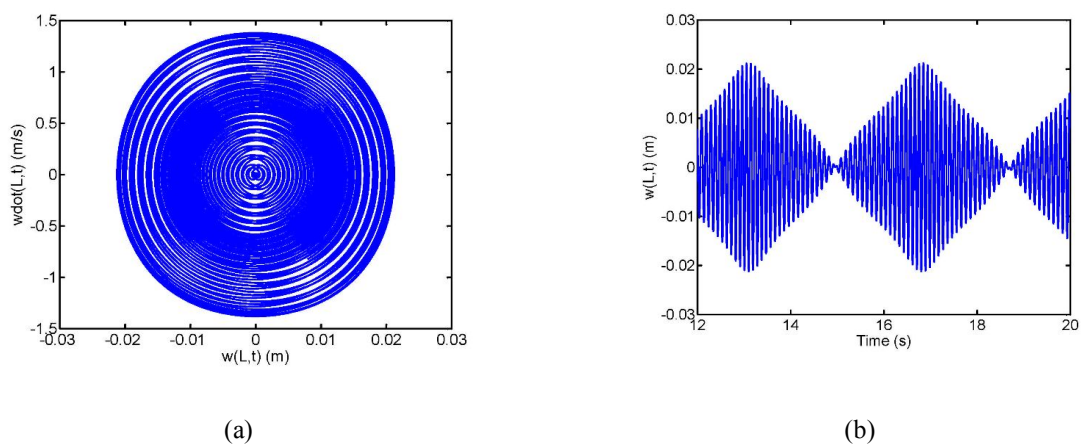


Fig. 6. (a) phase plane, (b) time history, (c) Poincare map, (d) power spectrum at $d_z = 0.177 m$.

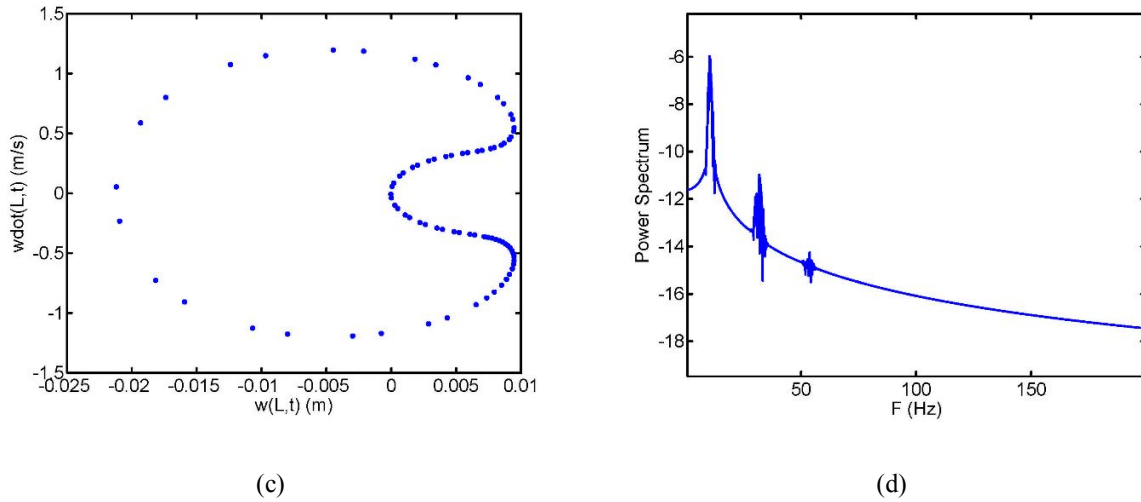


Fig. 6. (a) phase plane, (b) time history, (c) Poincare map, (d) power spectrum at $d_z = 0.177 m$.(Cont.)

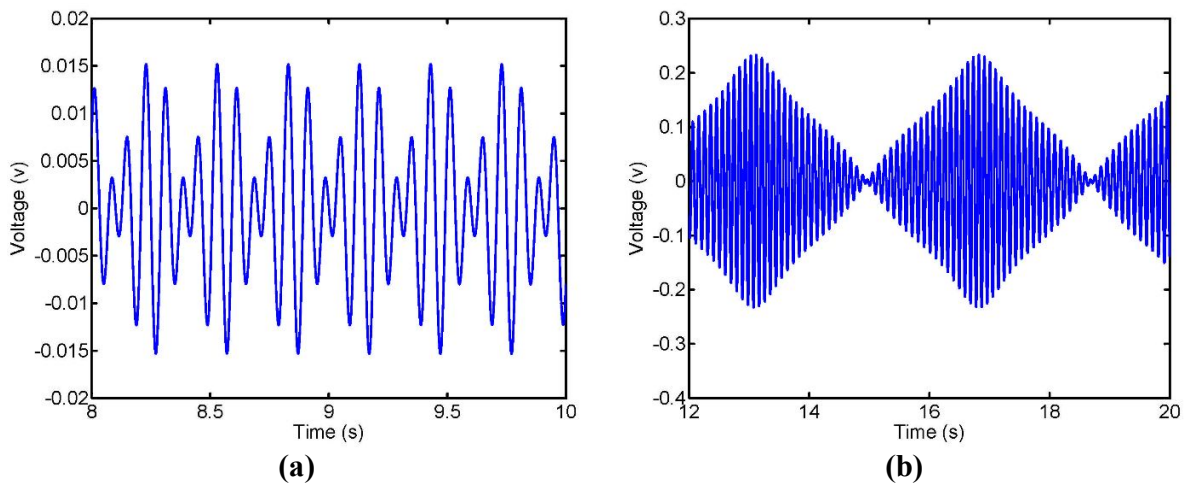


Fig. 7. Output voltage of energy harvesting system at (a) $d_z = 0.157 m$, (b) $d_z = 0.177 m$.

In the energy harvesting system, increasing the output voltage is the main goal in this regard. Fig 7 (a), shows the harvested voltage at $d_z = 0.157 m$. In this case, the maximum output is $0.0152V$. Fig 7 (b), shows the harvested voltage at $d_z = 0.177 m$. In this case, the maximum output is $0.233V$. These results show that, one can obtain higher voltage in the region $d_z = [0.138 \square 0.177] m$.

As showed in all aforementioned results, in some regions there were sudden increment in beam tip displacements; that has need to more explanation. According to equation (31), the main contribution of generalized forces is related to magnetic forces. Based on equations (11) to (18), these forces related to the gap distance between two external magnets and the separation distance between the tip and external magnets as well as the tip magnet height and length. So, by changing these parameters, the generalized forces may be affected. Fig. 8 shows typical generalized force versus magnet parameters.

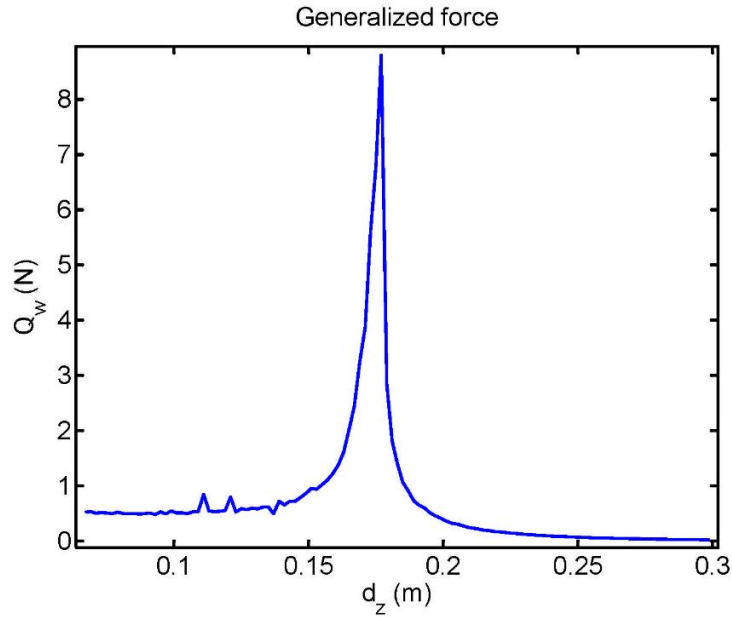


Fig. 8. Generalized force versus magnet gap distance d_z .

As illustrated in Fig. 8, the generalized forces mean value reach to 8.803 N at $d_z = 0.177\text{ m}$. This typical result confirms the significance of the magnetic force and moment on behavior of the system.

Also, the effect of exciting frequency on the beam tip displacement and the harvested voltage is investigated as a case study in Fig. 9. As depicted, the inherent frequency of the bimorph increases by decreasing the separation distance between two external magnets. Moreover, the higher voltage is harvested at small separation distances between the external magnets with higher exciting frequencies.

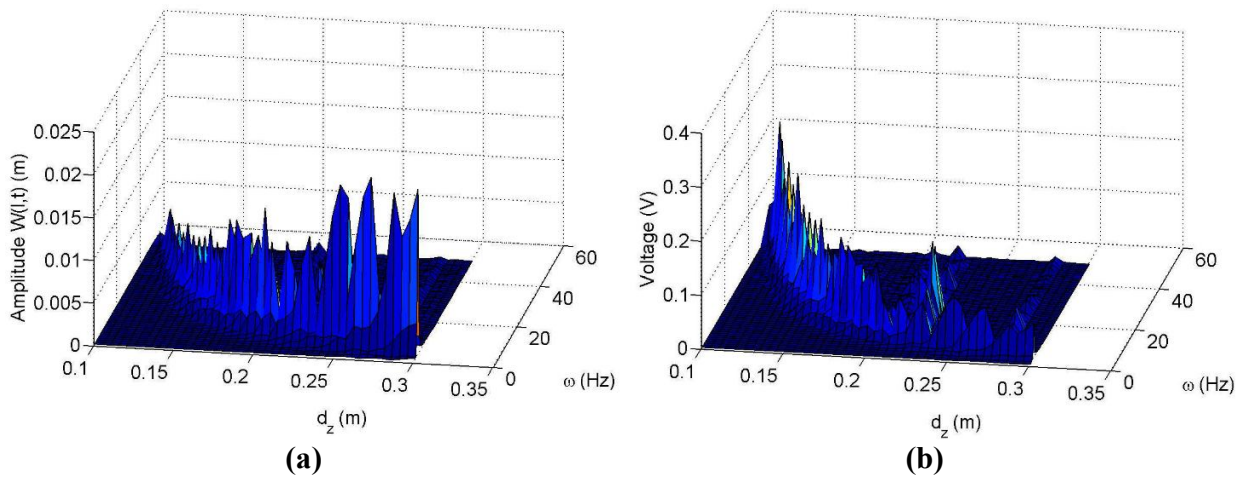


Fig. 9. Waterfall diagram: (a) amplitude, (b) voltage, versus magnets gap distance and frequency.

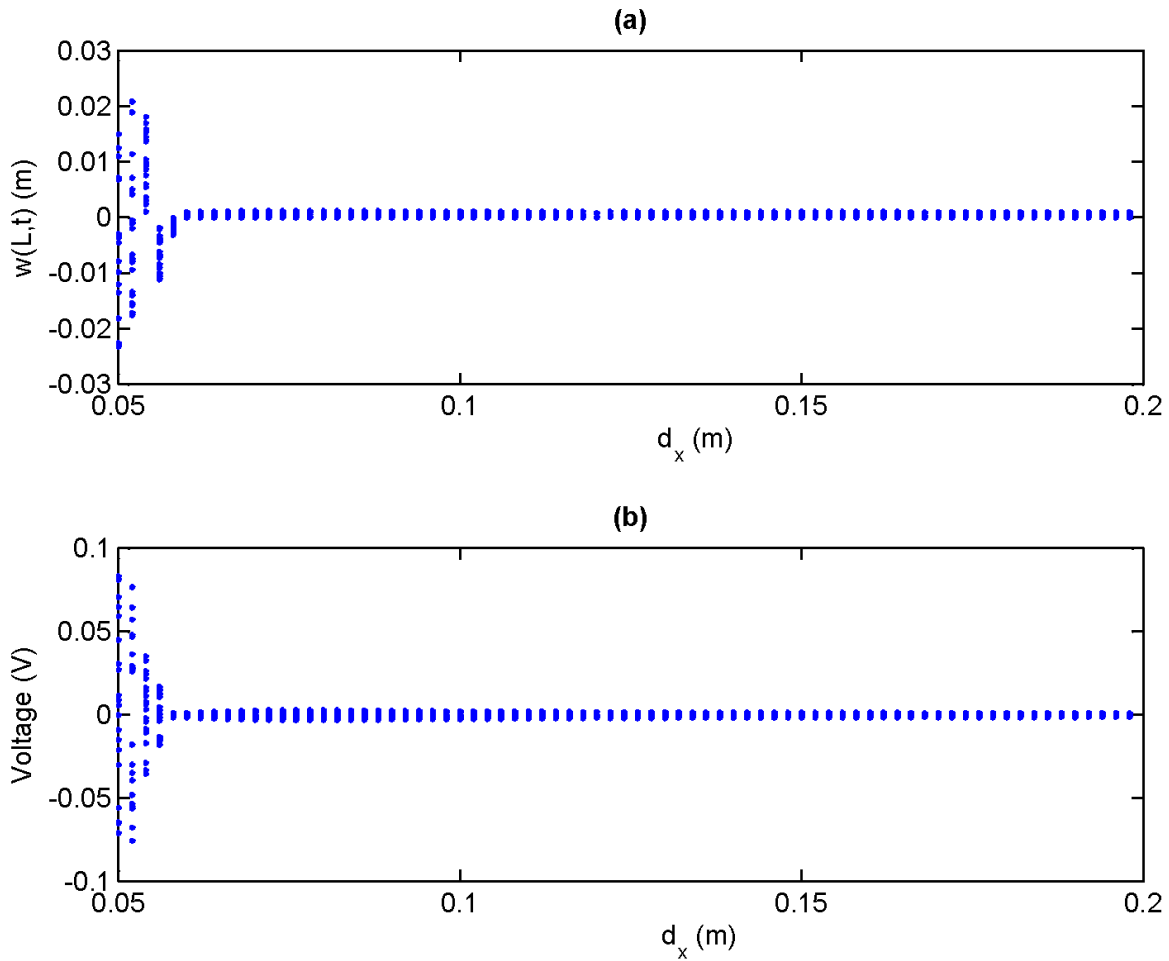


Fig. 10. Bifurcation diagrams (a) beam tip displacement, (b) voltage.

Fig. 10 shows the bifurcation diagrams of the beam tip displacement and harvested voltage versus d_x , the distance between tip and the external magnets. At $d_x = 0.05m$ the harvested voltage reach the maximum value about $0.1V$. In the small region of d_x , the tip displacement begin to increase, simultaneously the voltage decreases. Up to $d_x = 0.058m$ both the tip displacement and the voltage are decreases and the dynamic behavior is still chaotic. Hereafter, by increasing the separation distance, both the tip displacement and voltage values are not show considerable change. It should be noted that in the first region of the bifurcation diagram, Fig. 9(a), the behavior of the system is irregular. To confirm that the captured behavior of the system in irregular region is the quasi-periodic or chaotic; there is needs to considering the other identifying techniques.

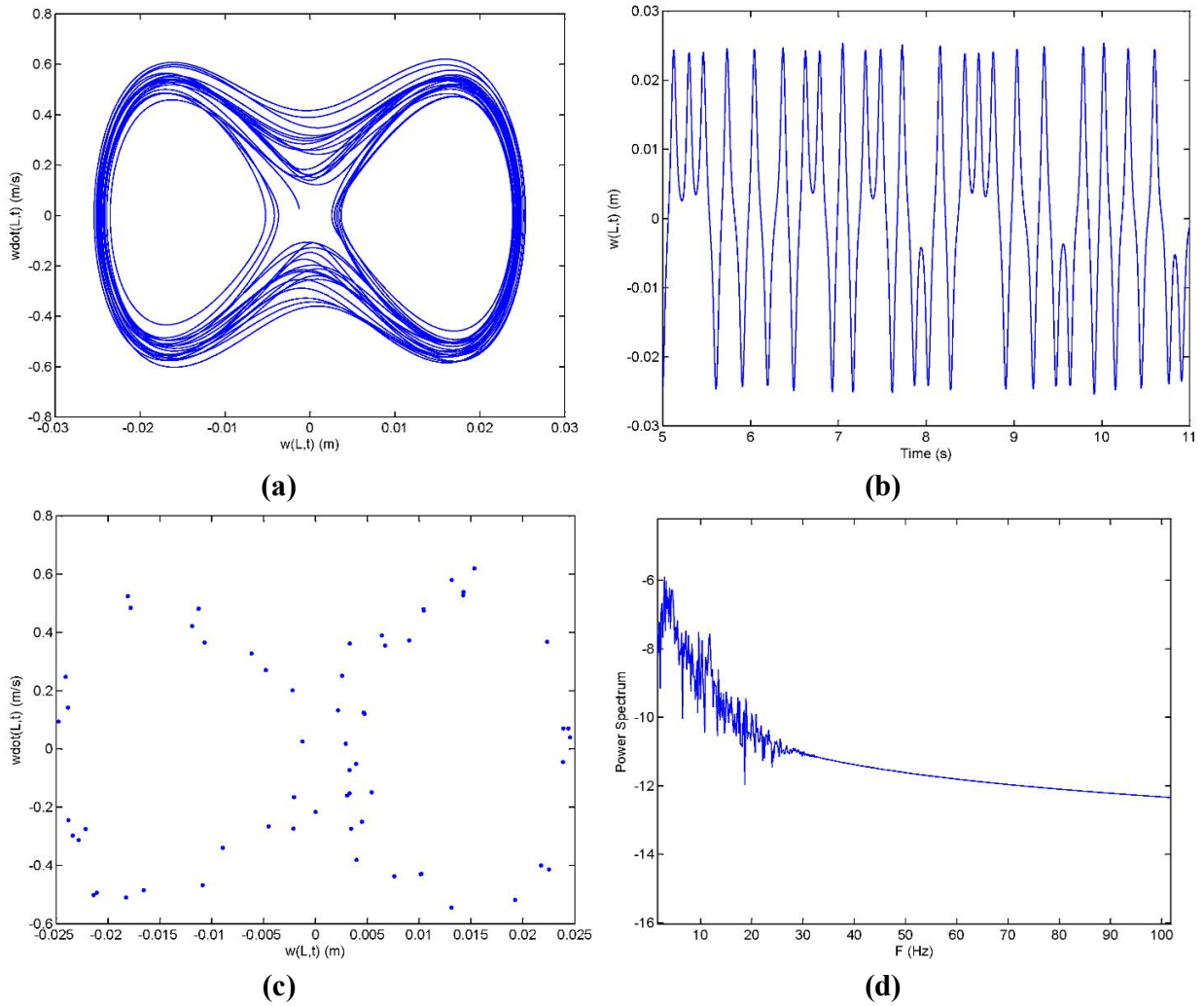


Fig. 11. (a) phase plane, (b) time history, (c) Poincare map, (d) power spectrum for $d_x = 0.05 m$

Fig.11 shows the behavior of the system at $d_x = 0.05 m$. As shown, the first region of bifurcation diagram is irregular. As depicted in Fig. 11, the phase plane shows many crossing and loops in some areas that confirms the chaotic behavior. The time history has not detectable amplitude and Poincare map does not form a closed curve and also the power spectrum has broad band nature, which confirms the chaotic behavior. Also Fig. 12, shows the chaotic behavior at $d_x = 0.056 m$, that is a typical point of high tip displacement in first region with lower voltage. Then, the simulation results with other points in the first region, $d_x = 0.05 m \square 0.058 m$, show that the dominant dynamic behavior of the system is chaotic for this case. However, one can capture the other dynamic behavior such as the sub-harmonic, periodic and quasi-periodic motions.

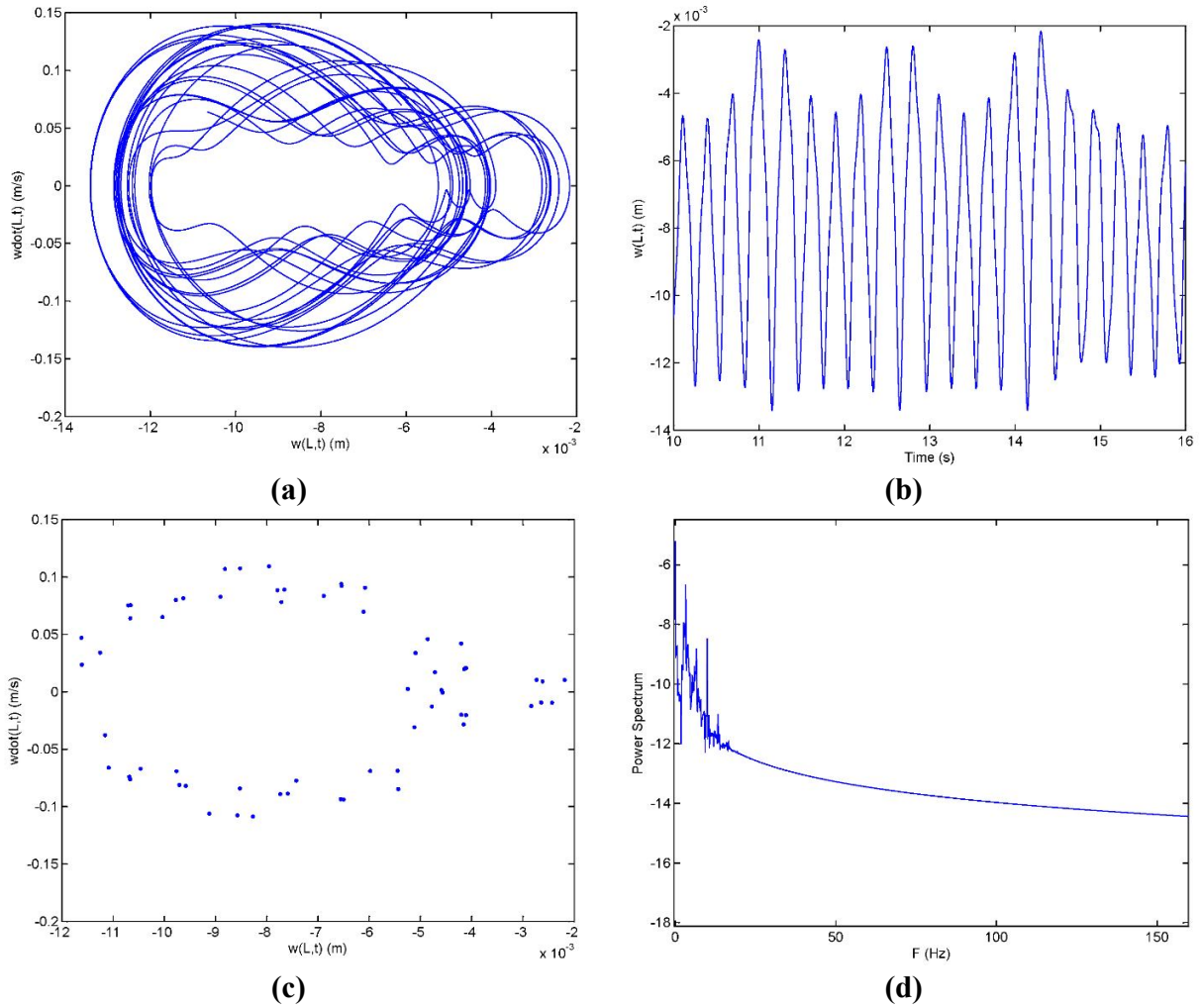


Fig. 12. (a) phase plane, (b) time history, (c) Poincare map, (d) power spectrum for $d_x = 0.056 m$.

The MLE also provide a useful means to detecting the chaotic behavior. By the MLE one can determine exponentially the average expansion or contraction rate of the deviation from initial direction $\mathbf{y}(0)$ on a trajectory of the system, which is given by $\bar{\lambda}_i = \lim_{t \rightarrow \infty} \frac{1}{t} \ln \left(\frac{\|\mathbf{y}(t)\|}{\|\mathbf{y}(0)\|} \right)$, where the symbol $\|\cdot\|$ denotes a vector norm and $\bar{\lambda}_i$ is the Lyapunov exponent (LE). By this definition, if any system contains at least one positive LE is defined as chaotic system. Fig 13 shows the MLE at two typical parameters. The maximum of LE is positive, that confirms the chaotic behavior at respective parameters.

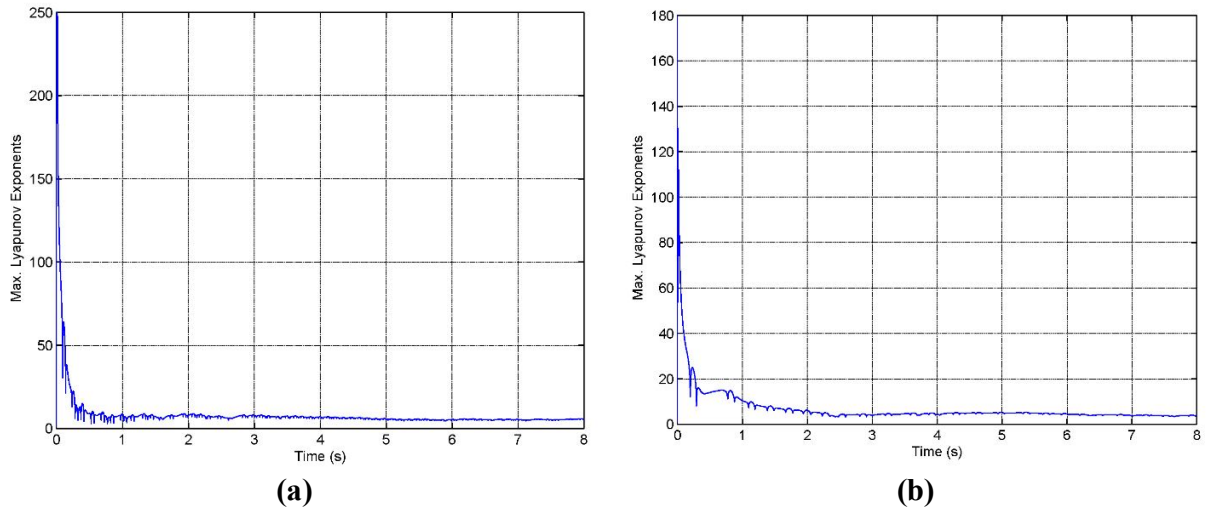


Fig. 13. MLE (maximum Lyapunov exponents) at (a) $d_x = 0.05\text{ m}$, (b) $d_x = 0.056\text{ m}$.

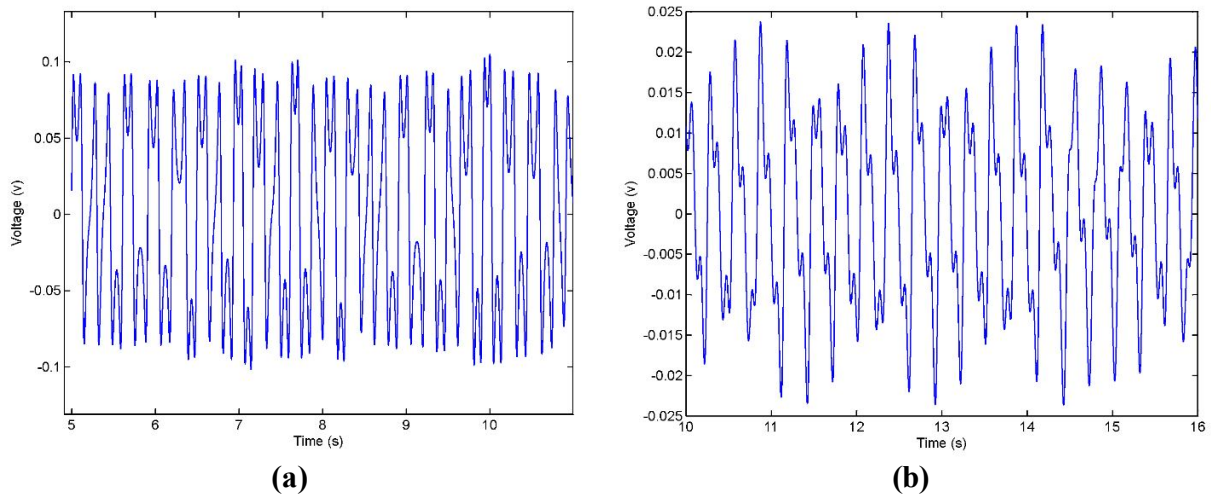


Fig. 14 .Output voltage of energy harvesting system at (a) $d_x = 0.05\text{ m}$, (b) $d_x = 0.056\text{ m}$.

Fig 14 (a), shows the harvested voltage at $d_x = 0.05\text{ m}$. In this case, the maximum output is 0.1048 V . Fig 14 (b), shows the harvested voltage at $d_x = 0.056\text{ m}$. In this case, the maximum output is 0.0237 V . However, the former point has very higher voltage than the second point. So by proper choosing the magnet gap distance, one can reach to optimum values of voltage in the small tip displacement.

3.2 .Effect of tip magnet dimensions

In this case, the bifurcation diagrams are obtained by changing the dimension of the tip magnet, height h_t and length L_t .

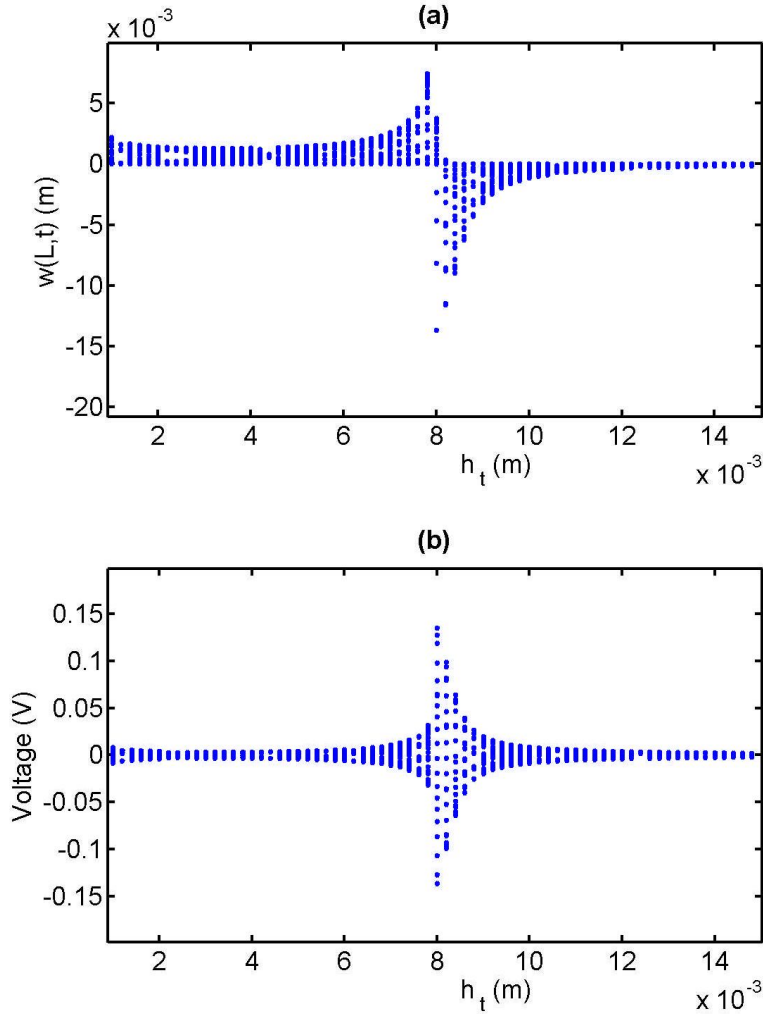


Fig. 15. Bifurcation diagrams (a) beam tip displacement, (b) voltage.

Fig. 15 shows the bifurcation diagram for the beam tip displacement and harvested voltage versus tip magnet height h_t . By increasing the magnet height up to $h_t = 0.006\text{ m}$, the tip displacement has not any considerable change and harvested voltage is low. Hereafter, both the tip displacement and the voltage begin to increasing up to $h_t = 0.0078\text{ m}$. In this point, the harvested voltage is about 0.032 V . At $h_t = 0.008\text{ m}$, there is a sudden change in displacement of the beam tip and the voltage. At this point, the harvested voltage value reach to 0.138 V . Hereafter, both the tip displacement and voltage begin to decreasing; that maintained up to $h_t = 0.0122\text{ m}$. In the end region of the bifurcation diagram, the tip displacements are very low and the generated voltage is not considerable. Dynamic behavior of the system in this case shows dominant the quasi-periodic behavior with the sub- or super-harmonic behaviors in some points. Dynamics of the system in this case shows dominant the quasi-periodic behavior with the sub- or super-harmonic behaviors at some points.

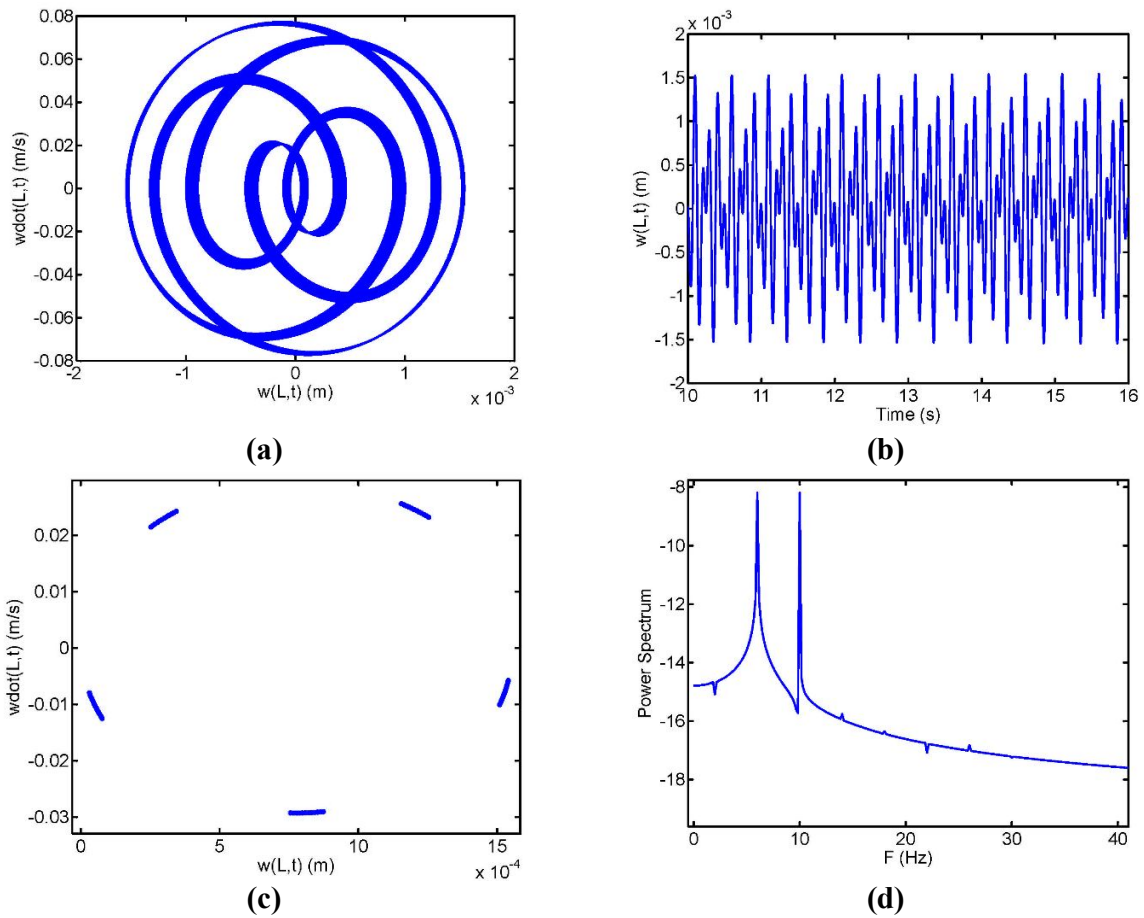


Fig. 16. (a) phase plane, (b) time history, (c) Poincare map, (d) power spectrum for $h_t = 0.0056 m$.

Fig. 16 illustrates the behavior of the system at $h_t = 0.0056 m$. At this value of h_t , the phase plane diagram is shown as definite closed circle. The time history has five detectible amplitude and Poincare map comprises five separate bands; also the power spectra shows some evident peaks amplitude before and after the exciting frequency (i.e. 2, 6; 14, 18; 22, 26), that confirm the sub-harmonic behavior with period five (5T). As shown in Fig. 17, at $h_t = 0.0078 m$, the phase plane show some crossing and loops that can be a sign of irregular motion. Since the time history has some definite peaks and Poincare map is closed curve, the power spectrum has some clear peaks around the main frequencies, the system behavior is quasi-periodic.

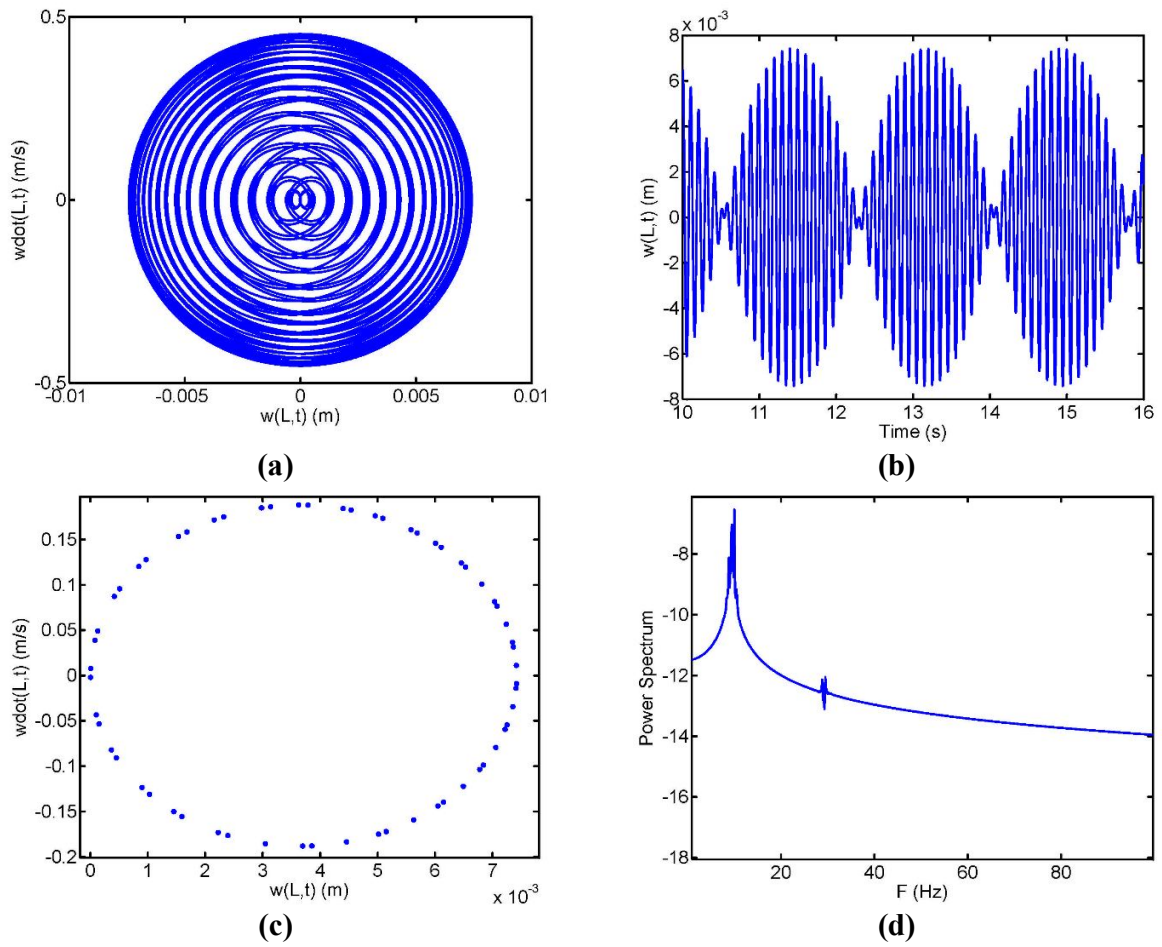


Fig. 17. (a) phase plane, (b) time history, (c) Poincare map, (d) power spectrum for $h_t = 0.0078 m$.

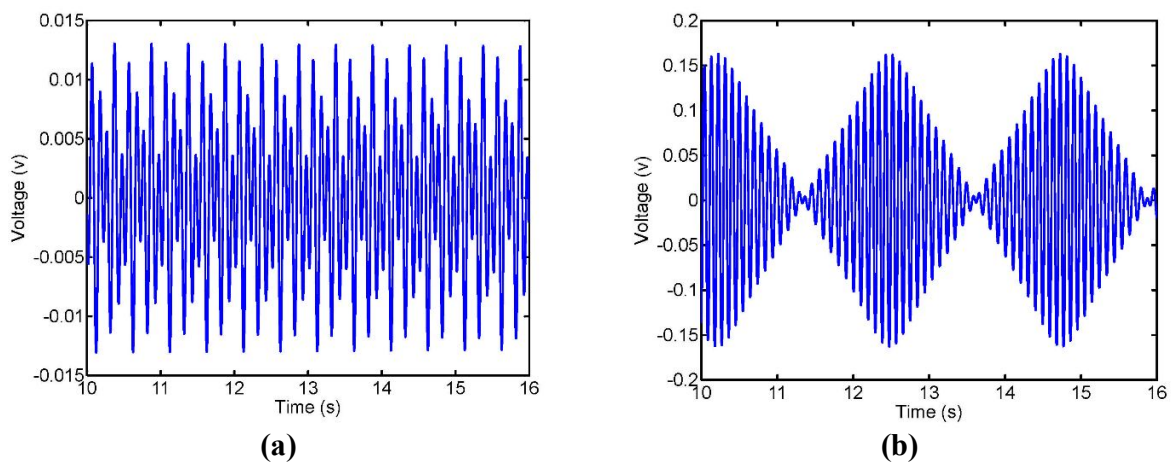


Fig. 18. Output voltage of energy harvesting system at (a) $h_t = 0.0056 m$, (b) $h_t = 0.008 m$.

Fig 18 (a), shows the harvested voltage at $h_t = 0.0056m$, where the maximum output voltage is $0.0131V$ and the maximum tip displacement is $0.15cm$. Fig 18 (b), shows the harvested voltage at $h_t = 0.008m$, where the maximum output is $0.163V$. These results show that there is not a wide region for increasing the harvested voltage when choosing the tip magnet height as a bifurcation parameter. However, there are some definite points for magnet height that results in higher voltages.

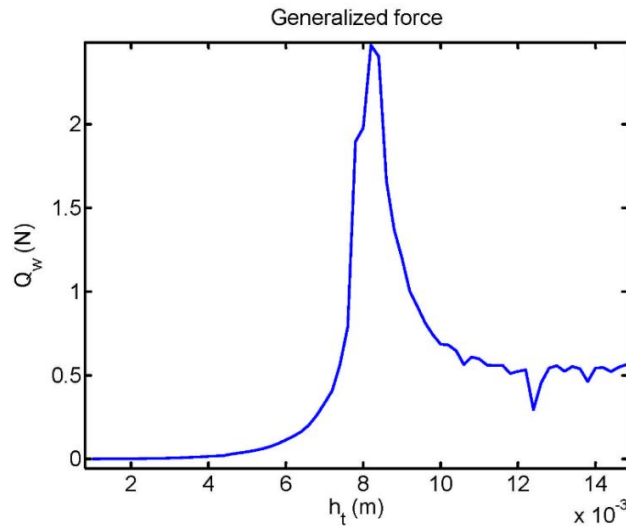


Fig. 19. Generalized force versus tip magnet height.

As illustrated in Fig. 19, for the tip magnet height $h_t = 0.0082m$, where the tip displacement is high, the generalized forces mean value is about $2.472N$ and before it, mean value of these forces is low. As before, this typical result also confirms the significance of the magnetic force and moment on behavior of the system.

Fig. 20 shows the bifurcation diagrams of the bimorph beam tip displacement and harvested voltage versus tip magnet length L_t . In this case, by increasing the tip magnet length, both the tip displacement and the voltage are gradually increases up to $L_t = 0.006m$, where the harvested voltage reach to $0.126V$. At $L_t = 0.0062m$, the tip displacement suddenly reversed but the generated voltage still has increasing nature. After this point, the harvested voltage is increases again up to $L_t = 0.0066m$ and reach to maximum value $0.217V$. At $L_t = 0.0068m$, there is a sudden decrease in the tip displacement and voltage. Hereafter, by changing L_t , both the tip displacement and voltage gradually decreases. In this case, the system behavior is contained irregular motion (quasi-periodic or chaotic) and the sub-harmonic motion in some points. As know, bifurcation diagrams give overall insight to system behavior. For detail information about the dynamic behavior and verifying the captured results by bifurcation diagram, other identifying techniques should be used. The following figures show the results in some typical points.

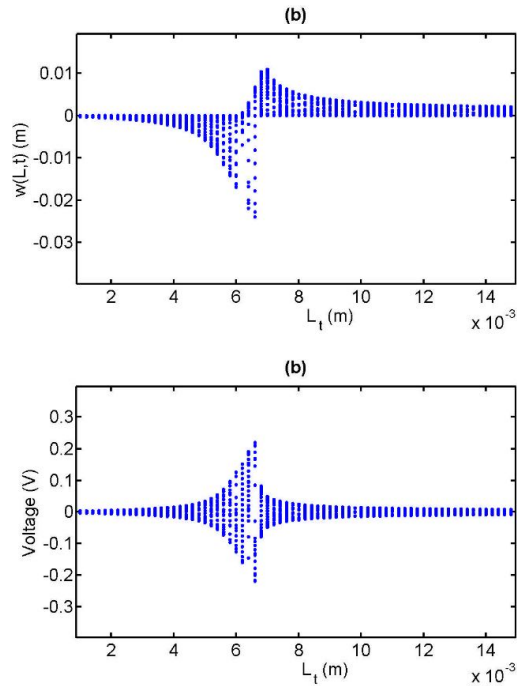


Fig. 20. Bifurcation diagram (a) beam tip displacement, (b) voltage.

Fig. 21 illustrates a typical behavior of the system at $L_t = 0.0098 m$. The time history has six detectible amplitude and Poincare section comprises six single points; also the power spectrum has an evident peak amplitude before (at 8.333 and 6.667) the main frequency, that confirms the sub-harmonic motion with period six ($6T$). Also Fig. 22 shows the behavior of the system at $L_t = 0.0134 m$, where the behavior of the system is sub-harmonic. The phase plane shows some finite closed curves that reveal the harmonic motion. Since the time history has four detectible amplitudes and the Poincare map is comprising four single points and also the power spectrum has clear peaks before main frequency at 7.5Hz and 5Hz, the system behavior is the sub-harmonic with period four ($4T$). The analysis with other points shows that the dominant behavior is quasi-periodic motion in this case.

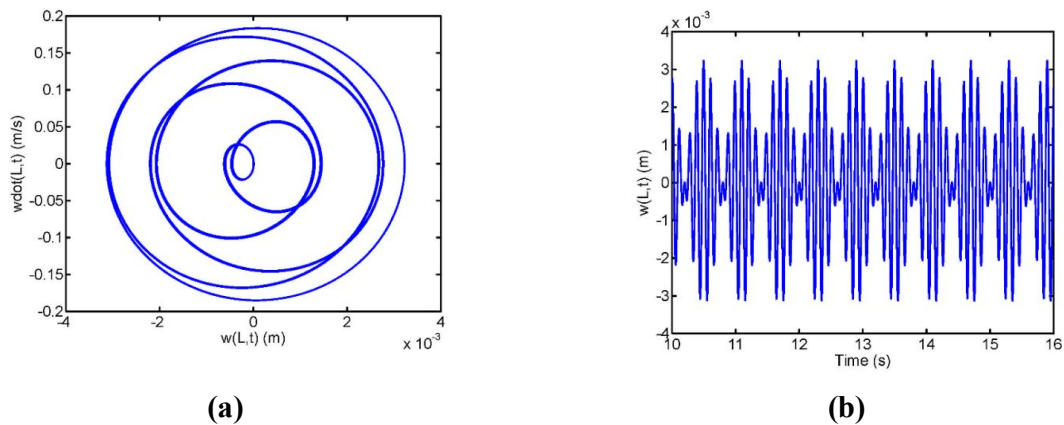


Fig. 21. (a) phase plane, (b) time history, (c) Poincare map, (d) power spectrum for $L_t = 0.0098 m$.

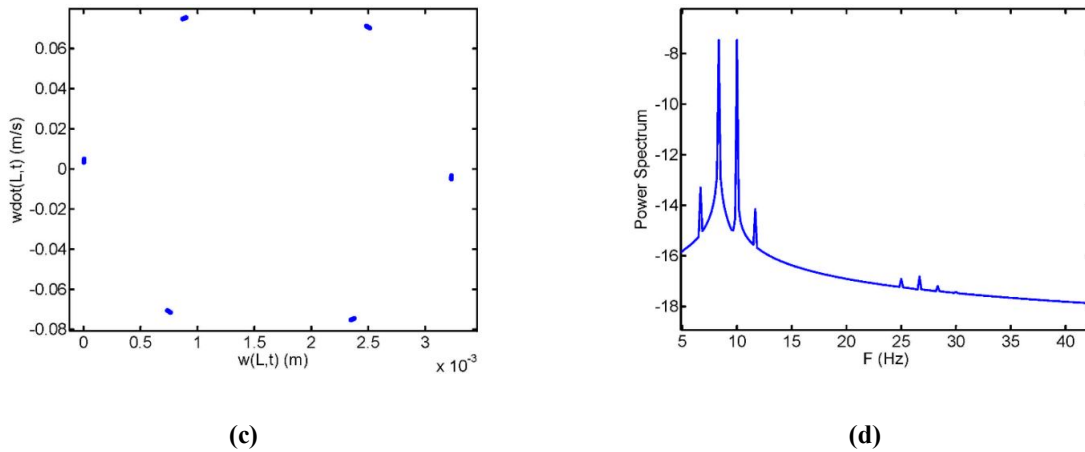


Fig. 21. (a) phase plane, (b) time history, (c) Poincare map, (d) power spectrum for $L_t = 0.0098 m$.(Cont.)

Finally, the harvested voltage in the end of the first region and begins of second region illustrated in Fig 23. At $L_t = 0.0066 m$, the harvested voltage is $0.263V$. At $L_t = 0.0068 m$, the maximum output voltage is $0.284V$. However, the maximum output voltage has been occurred in the end of the first and begins of the second regions of the bifurcation diagram. So, one can use suitable sections of two regions to reach the optimum energy value.

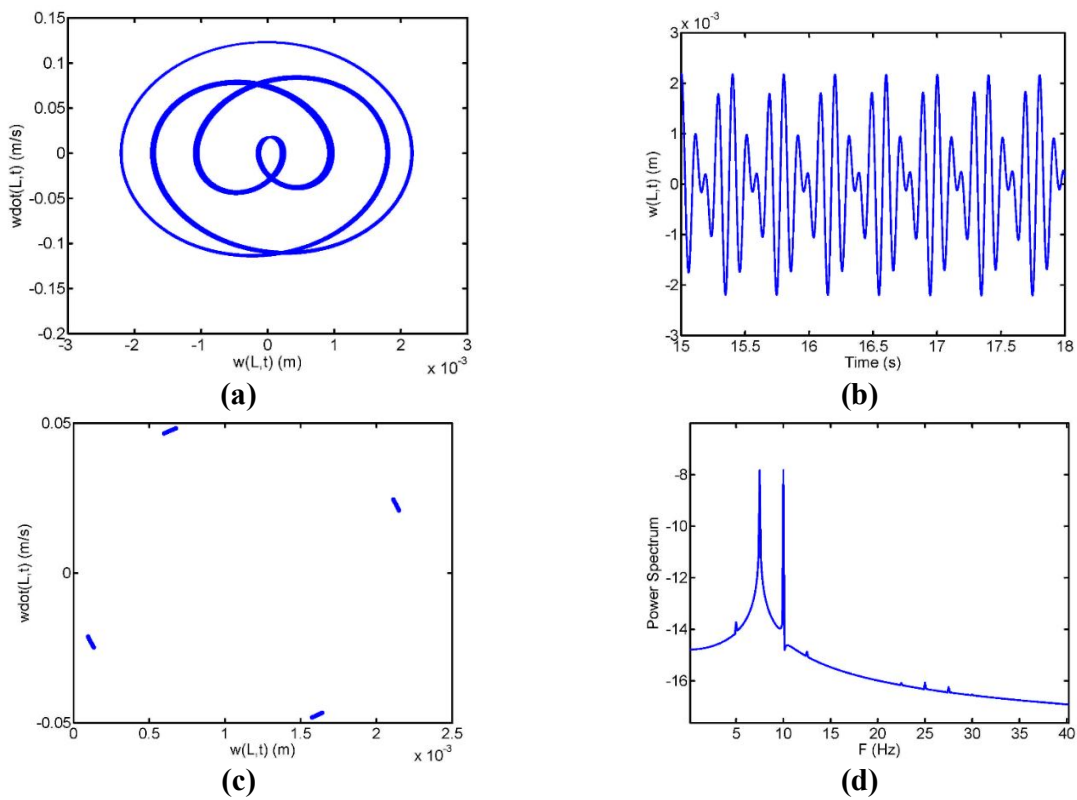


Fig. 22. (a) phase plane, (b) time history, (c) Poincare map, (d) power spectrum for $L_t = 0.0134 m$.

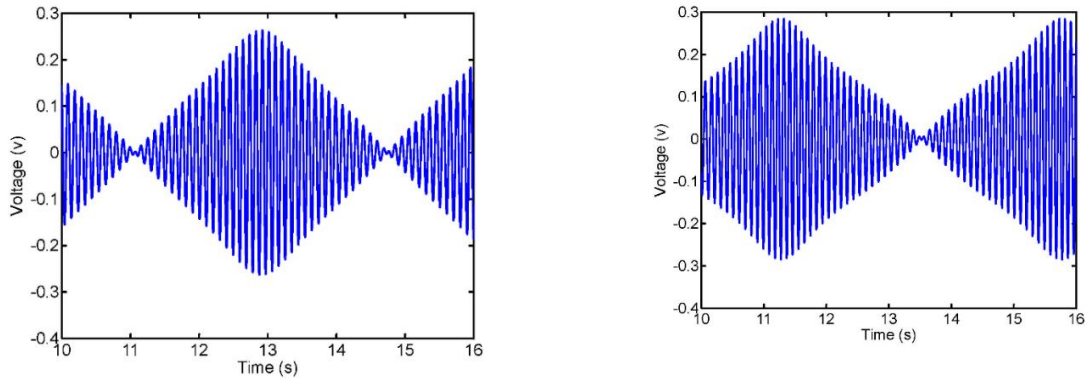


Fig. 23. Output voltage of energy harvesting system at (a) $L_t = 0.0066 m$, (b) $L_t = 0.0068 m$.

4. Conclusions

In this article, the influence of distances and dimensions of magnets on the nonlinear behavior and voltage level of a typical piezo-magneto-elastic bimorph was studied. The partial differential equations of the motion were discretized by using the assumed mode method. The number of modes effects analysis showed that for exciting frequencies lower than the first frequency of the system, only one assumed mode is to be sufficient for the numerical analysis. Also, the validity of the extracted model verified by previously published experimental results. The bifurcation diagrams were used to detect the nonlinear behaviors and the obtained results confirmed by using phase plane portrait, time history diagram, Poincare map, power spectra and Lyapunov exponents. The simulation results showed that by changing of the gap distance between the external magnets, the dominant nonlinear behavior of the system in irregular regions was quasi periodic. Also, by changing the separation distance of the tip magnet and the external magnets, the dominant nonlinear behavior of the system in irregular regions was chaotic. However, the effect of the separation distance of the tip and the external magnets on the output voltage is more than the effect of the external magnets gap distance. It can be due to this fact that, by changing the separation distance, the effects of magnetic field on beam tip deflections is more than the external magnets gap distance. Moreover, the effect of the tip magnet dimension on the nonlinear behavior of the bimorph was studied and the results showed that the dominant behavior of the bimorph in irregular regions was quasi periodic with relatively higher harvested voltage. In general, this system with the sub harmonic or super harmonic behaviors has minimum harvested voltage, whereas the irregular regions (chaotic or quasi-periodic) behaviors have maximum harvested voltage.

Appendix (A): Coefficients of Eqs. (25) – (27)

Based on the kinetic energy, Eq. (25), the following terms are defined

$$\begin{aligned}
 M_{ij}^k &= \int_{V_k} \rho_s [\psi_i'(x)\psi_j'(x)z^2 + \psi_i(x)\psi_j(x)] dV_k \quad (k = s, p_1, p_2) \\
 H_i^k &= \int_{V_k} \rho_k \psi_i(x) dV_k \quad (k = s, p_1, p_2) \\
 M_{ij}^L &= M \psi_i(L)\psi_j(L) \\
 M_{ij}^I &= I_M \psi_i'(L)\psi_j'(L) \\
 H_i^L &= 2\psi_i(L) \\
 m_T &= m_s + m_{p_1} + m_{p_2} + M
 \end{aligned} \tag{A.1}$$

Therefore, the elements of matrix \mathbf{M} and vector \mathbf{H} are given as

$$\begin{aligned}
 M_{ij} &= M_{ij}^s + M_{ij}^{p_1} + M_{ij}^{p_2} + M_{ij}^L + M_{ij}^I \\
 H_i &= H_i^s + H_i^{p_1} + H_i^{p_2}
 \end{aligned} \tag{A.2}$$

Based on the strain potential energy, Eq. (26), the following terms are defined

$$\begin{aligned}
 K_{ij}^k &= \int_{V_k} E_k z^2 \psi_i''(x)\psi_j''(x) dV_k \quad (k = s, p_1, p_2) \\
 G_i^k &= \frac{1}{2} \int_{V_k} e_{31} z \psi_i''(x) dV_k \quad (k = p_1, p_2)
 \end{aligned} \tag{A.3}$$

Therefore, the elements of matrix \mathbf{K} and vector \mathbf{G} are given as

$$\begin{aligned}
 K_{ij} &= K_{ij}^s + K_{ij}^{p_1} + K_{ij}^{p_2} \\
 G_i &= G_i^{p_1} + G_i^{p_2}
 \end{aligned} \tag{A.4}$$

Also, the virtual work of the electromechanical system, Eq. (19), is written as follows

$$\delta W_{nc} = \left(\int_0^t \frac{v}{R_L} dt \right) \delta v + [f_{M_z} \boldsymbol{\psi}(L) + \tau_M \boldsymbol{\psi}'(L)]^T \delta \mathbf{q} \tag{A.5}$$

Therefore, the generalized forces and the output electric charge of the piezoelectric layers are given as

$$\begin{aligned}
 Q_F &= f_{M_z} \boldsymbol{\psi}(L) + \tau_M \boldsymbol{\psi}'(L) \\
 Q_E &= \int_0^t \frac{v}{R_L} dt
 \end{aligned} \tag{A.6}$$

References

- [1] M. Umeda, K. Nakamura, S. Ueha, Analysis of the transformation of mechanical impact energy to electric energy using piezoelectric vibrator, Japanese Journal of Applied Physics, 35 (1996) 3267.
- [2] G.R. Samuel, Analysis of energy harvesting positive displacement motor, Journal of Energy Resources Technology, 129 (2007) 360-363.
- [3] N.E. DuToit, B.L. Wardle, Experimental verification of models for microfabricated piezoelectric vibration energy harvesters, AIAA journal, 45 (2007) 1126-1137.

- [4] X.d. Xie, Q. Wang, A mathematical model for piezoelectric ring energy harvesting technology from vehicle tires, *International Journal of Engineering Science*, 94 (2015) 113-127.
- [5] N.V. Satpute, S.N. Satpute, L.M. Jugulkar, Hybrid electromagnetic shock absorber for energy harvesting in a vehicle suspension, *Proceedings of the Institution of Mechanical Engineers, Part C: Journal of Mechanical Engineering Science*, 10 (2016) 1-18.
- [6] A. Abdelkefi, Aeroelastic energy harvesting: A review, *International Journal of Engineering Science*, 100 (2016) 112-135.
- [7] M. Nouh, O. Aldraihem, A. Baz, Onset of Oscillations in Traveling Wave Thermo-Acoustic-Piezo-Electric Harvesters Using Circuit Analogy and SPICE Modeling, *Journal of Dynamic Systems, Measurement, and Control*, 136 (2014) 1-10.
- [8] M. Mohammadpour, M. Dardel, M.H. Ghasemi, M.H. Pashaei, Nonlinear energy harvesting through a multimodal electro-mechanical system, *Journal of Theoretical and Applied Vibration and Acoustics*, 1 (2015) 73-84.
- [9] S.-J. Jang, I.-H. Kim, K. Park, H.-J. Jung, An enhanced tunable rotational energy harvester with variable stiffness system for low-frequency vibration, *Proceedings of the Institution of Mechanical Engineers, Part C: Journal of Mechanical Engineering Science*, 230 (2016) 732-736.
- [10] P. Harte, E. Blokhina, O. Feely, D. Fournier-Prunaret, D. Galayko, Electrostatic vibration energy harvesters with linear and nonlinear resonators, *International Journal of Bifurcation and Chaos*, 24 (2014) 1430030.
- [11] A. Erturk, D.J. Inman, *Piezoelectric energy harvesting*, John Wiley & Sons, 2011.
- [12] S. Roundy, P.K. Wright, A piezoelectric vibration based generator for wireless electronics, *Smart Materials and structures*, 13 (2004) 1131-1144.
- [13] N.E. Dutoit, B.L. Wardle, S.G. Kim, Design considerations for MEMS-scale piezoelectric mechanical vibration energy harvesters, *Integrated ferroelectrics*, 71 (2005) 121-160.
- [14] N.W. Hagood, W.H. Chung, A. Von Flotow, Modelling of piezoelectric actuator dynamics for active structural control, *Journal of intelligent material systems and structures*, 1 (1990) 327-354.
- [15] H.A. Sodano, G. Park, D.J. Inman, Estimation of electric charge output for piezoelectric energy harvesting, *Strain*, 40 (2004) 49-58.
- [16] A. Erturk, D.J. Inman, Issues in mathematical modeling of piezoelectric energy harvesters, *Smart Materials and Structures*, 17 (2008) 065016.
- [17] A. Erturk, D.J. Inman, A distributed parameter electromechanical model for cantilevered piezoelectric energy harvesters, *Journal of vibration and acoustics*, 130 (2008) 041002.
- [18] A. Erturk, D.J. Inman, An experimentally validated bimorph cantilever model for piezoelectric energy harvesting from base excitations, *Smart materials and structures*, 18 (2009) 025009.
- [19] C.D.M. Jr., A. turk, D.J. Inman, An electromechanical finite element model for piezoelectric energy harvester plates, *Journal of Sound and Vibration*, 327 (2009) 9-25.
- [20] N.G. Elvin, A.A. Elvin, A coupled finite element—circuit simulation model for analyzing piezoelectric energy generators, *Journal of Intelligent Material Systems and Structures*, 20 (2009) 587-595.
- [21] S. Zhao, A. Erturk, Electroelastic modeling and experimental validations of piezoelectric energy harvesting from broadband random vibrations of cantilevered bimorphs, *Smart Materials and Structures*, 22 (2012) 015002.
- [22] S.C. Stanton, A. Erturk, B.P. Mann, D.J. Inman, Nonlinear piezoelectricity in electroelastic energy harvesters: modeling and experimental identification, *Journal of Applied Physics*, 108 (2010) 074903.
- [23] A. Abdelkefi, A.H. Nayfeh, M.R. Hajj, Global nonlinear distributed-parameter model of parametrically excited piezoelectric energy harvesters, *Nonlinear Dynamics*, 67 (2012) 1147-1160.
- [24] M. Ferrari, V. Ferrari, M. Guizzetti, D. Marioli, A single-magnet nonlinear piezoelectric converter for enhanced energy harvesting from random vibrations, *Procedia Engineering*, 5 (2010) 1156-1159.
- [25] M. Ferrari, V. Ferrari, M. Guizzetti, B. Andò, S. Baglio, C. Trigona, Improved energy harvesting from wideband vibrations by nonlinear piezoelectric converters, *Sensors and Actuators A: Physical*, 162 (2010) 425-431.
- [26] A. Triplett, D.D. Quinn, The effect of non-linear piezoelectric coupling on vibration-based energy harvesting, *Journal of Intelligent Material Systems and Structures*, 20 (2009) 1959-1967.
- [27] R. Masana, M.F. Daqaq, Relative performance of a vibratory energy harvester in mono- and bi-stable potentials, *Journal of Sound and Vibration*, 330 (2011) 6036-6052.
- [28] R. Masana, M.F. Daqaq, Energy harvesting in the super-harmonic frequency region of a twin-well oscillator, *Journal of Applied Physics*, 111 (2012) 044501.
- [29] B.P. Mann, D.A. Barton, B.A. Owens, Uncertainty in performance for linear and nonlinear energy harvesting strategies, *Journal of Intelligent Material Systems and Structures*, 23 (2012) 1451-1460.

- [30] M.F. Daqaq, R. Masana, A. Erturk, D.D. Quinn, On the role of nonlinearities in vibratory energy harvesting: a critical review and discussion, *Applied Mechanics Reviews*, 66 (2014) 040801.
- [31] A.J. Sneller, P. Cette, B.P. Mann, Experimental investigation of a post-buckled piezoelectric beam with an attached central mass used to harvest energy, *Proceedings of the Institution of Mechanical Engineers, Part I: Journal of Systems and Control Engineering*, 225 (2011) 497-509.
- [32] M. Coccolo, G. Litak, J.M. Seoane, M.A.F. Sanjuán, Energy harvesting enhancement by vibrational resonance, *International Journal of Bifurcation and Chaos*, 24 (2014) 1430019.
- [33] M. Coccolo, G. Litak, J.M. Seoane, M.A.F. Sanjuán, Optimizing the electrical power in an energy harvesting system, *International Journal of Bifurcation and Chaos*, 25 (2015) 1550171.
- [34] R.L. Harne, K.W. Wang, Axial suspension compliance and compression for enhancing performance of a nonlinear vibration energy harvesting beam system, *Journal of Vibration and Acoustics*, 138 (2016) 011004.
- [35] J. Cao, S. Zhou, D.J. Inman, J. Lin, Nonlinear dynamic characteristics of variable inclination magnetically coupled piezoelectric energy harvesters, *Journal of Vibration and Acoustics*, 137 (2015) 021015.
- [36] G. Caruso, Broadband energy harvesting from vibrations using magnetic transduction, *Journal of Vibration and Acoustics*, 137 (2015) 064503.
- [37] P. Firoozy, S.E. Khadem, S.M. Pourkiaee, Broadband energy harvesting using nonlinear vibrations of a magnetopiezoelectric cantilever beam, *International Journal of Engineering Science*, 111 (2017) 113-133.
- [38] T. Yildirim, M.H. Ghayesh, W. Li, G. Alici, A Nonlinearly Broadband Tuneable Energy Harvester, *Journal of Dynamic Systems, Measurement, and Control*, 139 (2017) 011008.
- [39] T. Yildirim, M.H. Ghayesh, T. Searle, W. Li, G. Alici, A parametrically broadband nonlinear energy harvester, *Journal of Energy Resources Technology*, 139 (2017) 032001.
- [40] D. Geiyer, J.L. Kauffman, Chaotification as a means of broadband energy harvesting with piezoelectric materials, *Journal of Vibration and Acoustics*, 137 (2015) 051005.
- [41] J.J. Abbott, O. Ergeneman, M.P. Kummer, A.M. Hirt, B.J. Nelson, Modeling magnetic torque and force for controlled manipulation of soft-magnetic bodies, *IEEE Transactions on Robotics*, 23 (2007) 1247-1252.
- [42] K. Yung, P. Landecker, D. Villani, An analytic solution for the force between two magnetic dipoles, *Physical Separation in Science and Engineering*, 9 (1998) 39-52.
- [43] M. Beleggia, M. De Graef, Y.T. Millev, The equivalent ellipsoid of a magnetized body, *Journal of Physics D: Applied Physics*, 39 (2006) 891-899.
- [44] D.J. Griffiths, *Introduction to electrodynamics*, in, 4th ed. Ltd., Publication, Prentice Hall 2013.
- [45] P. Kim, J. Seok, A multi-stable energy harvester: Dynamic modeling and bifurcation analysis, *Journal of Sound and Vibration*, 333 (2014) 5525-5547.